Journal of Molecular Liquids 244 (2017) 241–251

Contents lists available at ScienceDirect

Journal of Molecular Liquids

journal homepage: www.elsevier.com/locate/molliq

Electronic structure, FT-IR analysis and nematic behaviour studies of para-methoxybenzylidine *p*-ethylaniline: Ab-initio and DFT approach

Sugriva Nath Tiwari [1], Dipendra Sharma *

Department of Physics, D.D.U. Gorakhpur University, Gorakhpur 273009, India

ARTICLE INFO

Article history:
Received 23 April 2017
Received in revised form 16 July 2017
Accepted 26 August 2017
Available online 30 August 2017

Keywords:
Nematic liquid crystal
PES
MEP
HOMO
LUMO
IR spectrum
Interaction energy

ABSTRACT

Electronic structure of para-methoxybenzylidine *p*-ethylaniline (MBEA), a pure nematic liquid crystal has been examined using ab–initio, HF/6-31G(d,p) and DFT B3LYP/6-31G(d,p) techniques with GAMESS program. MBEA transforms from crystal to nematic at 28 °C and nematic to isotropic phase at 57 °C. Potential Energy Surface (PES) in terms of various conformations and charge distribution analysis have been carried out. Molecular Electrostatic Potential (MEP), Highest Occupied Molecular Orbital (HOMO) and Lowest Unoccupied Molecular Orbital (LUMO) surfaces have been scanned. Ionization potential, electron affinity, electronegativity, global hardness and softness parameters of the liquid crystal molecule have been determined. Molecular and thermodynamic properties such as total energy, dipole moment, entropy, enthalpy and Gibbs free energy have been calculated at 298.15 K temperature. FTIR showed that calculated and experimental frequencies are in agreement. Stacking, side by side and end to end interactions between a molecular pair have been evaluated employing modified second order perturbation theory along with multicentred-multipole expansion technique. Results have been used to elucidate the physico-chemical and liquid crystalline properties of the system.

1. Introduction

In a few decades, computer simulation methods have emerged as powerful tool for observation and determination of various physical and chemical prospects of molecular systems in response to conditions that cannot be easily applied through experimental techniques [1,2]. Now a days, computer simulation modeling assists in all the disciplines e.g. in design, creation and evaluation of materials having complex molecular arrangements [3]. Materials in nature are divided into different phases depending upon the mobility of individual atoms or molecules. Apart from the three familiar states e.g. solid, liquid and gas, there exist a large number of other intermediate phases. An important intermediate phase is formed by liquid crystals, which exhibit features from both solid and liquid states. Liquid crystals possess the ordering properties of solids but they flow like liquids [4,5]. Many molecules and macromolecules present in nature exhibit liquid crystalline state under suitable conditions. A slight change in composition and/or in the physical/chemical properties can materially offset the formation, continuation and cessation of the mesomorphic state - a delicate balance characteristics of living processes [6]. At present, liquid crystals have emerged as beautiful, mysterious and soft condensed materials. Since the topic of liquid crystals is very interesting and it encapsulates physics, chemistry and in some aspect also biology; it constitutes a very suitable content for an interdisciplinary integration of the natural science studies [7].

Molecules having geometrical anisotropy and high polarizability may exhibit one or more liquid crystalline phases. Moieties incorporated into the main chain or side group in a molecule can result in the formation of liquid crystalline phase at moderate or high temperatures. The formation of such a phase and its type are closely related to the molecular structure [8]. Therefore, to correlate the molecular structure with liquid crystallinity at the molecular level still remains an elusive goal [9]. Further, nature and strength of various types of molecular interactions acting between sides, planes and ends of a pair of molecules, solely govern the liquid crystalline behaviour of molecules. Based upon semi-empirical and quantum mechanical techniques, molecular interactions in several mesogenic compounds have been studied [9–13]. The availability of high speed computers has facilitated the understanding of liquid crystalline properties through computer simulation, modeling and quantum chemical studies. Further, MEP, HOMO and LUMO studies are also being used as tools for the study of molecular reactivity, charge transfer, interactions, electro-optical and other molecular properties of liquid crystals [9,14–16].

* Corresponding author at: Department of Physics, D.D.U. Gorakhpur University, Gorakhpur, India.
E-mail addresses: sntiwari123@rediffmail.com (S.N. Tiwari), d_11sharma@rediffmail.com (D. Sharma).
[1] Department of Physics, D.D.U. Gorakhpur University, Gorakhpur, India-273009.

http://dx.doi.org/10.1016/j.molliq.2017.08.098
0167-7322/

In view of the above facts, the present paper deals with the geometry, conformation, MEP surface, HOMO and LUMO analysis of the MBEA molecule based upon ab-initio and DFT studies. Results have been used to understand the physico-chemical and liquid crystalline behaviour of the molecule.

2. Theoretical method

The molecular structure of MBEA has been optimized by both ab-initio (RHF) and density functional theory (B3LYP) methods with 6-31G(d,p) basis set. The exchange correlation energy used in density functional theory is of the following form:

$$E_{XC} = (1-a_0)E_X^{LSDA} + a_0E_X^{HF} + a_X\Delta E_X^{B88} + a_CE_C^{LYP} + (1-a_C)E_C^{VWN} \quad (1)$$

where the energy terms used are the Slater exchange, the Harree-Fock exchange, Becke's exchange functional correction, the gradient corrected correlation functional of Lee, Parr, Yang and the local correlation functional of Vosco, Wilk and Nusair [17].

2.1. Conformational, molecular electrostatic potential and HOMO-LUMO surface study

The maps of electrostatic potential are being used in scientific research for over fifty years [18]. The potential energy surface (PES) is a multi-dimensional surface on which each energy point corresponds to a possible configuration of the system [19]. At PES, there are several regions where the system spends most of its time. Those regions are usually local minima or low energy areas corresponding to stable system configurations. From the view of dynamics on the PES, system usually vibrates around those local minima, while it occasionally hops from one local minimum to another.

Geometry optimization and computation of net charge at each atomic centre of the molecule have been carried out using ab-initio HF/6-31G(d,p) and DFT B3LYP/6-31G(d,p) methods with GAMESS program [20]. Further, molecular electrostatic potential (MEP) and HOMO-LUMO surfaces of the optimized MBEA molecule have been scanned [21,22]. Molecular properties like ionization potential (I), electron affinity (A), electronegativity (χ), global hardness (η) and softness (S) have been calculated.

Relation between chemical potential (μ) and electronegativity (χ) established by Parr et al. [23] is given by the relation:

$$\mu = \left(\frac{\partial E}{\partial N}\right)_{v(r)} = -\chi \quad (2)$$

where $v(r)$ and μ are the external and electronic chemical potentials respectively. Ionization potential (I), electron affinity (A), electronegativity (χ), global hardness (η) and softness (S) parameters are defined in terms of the energy of the HOMO and the LUMO using Koopman's theorem [24]. Ionization potential (I) and electron affinity (A) [25] are given as:

$$I = -E_{HOMO} \quad \text{and} \quad A = -E_{LUMO} \quad (3)$$

Using the values of I and A, one can determine electronegativity (χ) [26] and the global hardness (η) [27] of the molecule:

$$\chi = \frac{I+A}{2} \quad and \quad \eta = \frac{I-A}{2} \quad (4)$$

Chemical softness (S) [26] and electrophilicity index (ω) which was proposed by Parr et al. [28] are given as:

$$S = \frac{1}{\eta} \quad and \quad \omega = \frac{\mu^2}{2\eta} \quad (5)$$

2.2. Vibrational assignment analysis

The vibrational frequencies have been theoretically determined using ab-inito HF/6-31G(d,p) and DFT B3LYP/6-31G(d,p) methods. The computed frequencies with significant intensities as compared with the experimental data are listed in Table 5.

2.3. Interaction energy study

According to the energy decomposition obtained by perturbation treatment, the total interaction energy (E_{TOTAL}) between two molecules is expressed as [29]:

$$E_{TOTAL} = E_{ELE} + E_{POL} + E_{DISP} + E_{REP} \quad (6)$$

where E_{ELE}, E_{POL}, E_{DISP} and E_{REP} represent electrostatic, polarization, dispersion and repulsion energy components respectively. Using multicentered-multipole expansion method [30], the electrostatic energy term is expressed as:

$$E_{ELE} = E_{QQ} + E_{QMI} + E_{MIMI} + - - - - - - - - \quad (7)$$

where E_{QQ}, E_{QMI} and E_{MIMI} etc. represent monopole-monopole, monopole-dipole, dipole-dipole and interaction energy terms consisting of multipoles of higher orders respectively. However, consideration up to the first three terms has been found to be sufficient for most of the molecular interaction problems [31]. Details of the mathematical treatment may be found in literature [10–12,29,32].

3. Results and discussion

3.1. Geometrical, conformational and Mulliken population analysis

As optimized by DFT method with B3LYP/6–31G(d,p) basis set, the molecular geometry of MBEA molecule is shown in Fig. 1; while

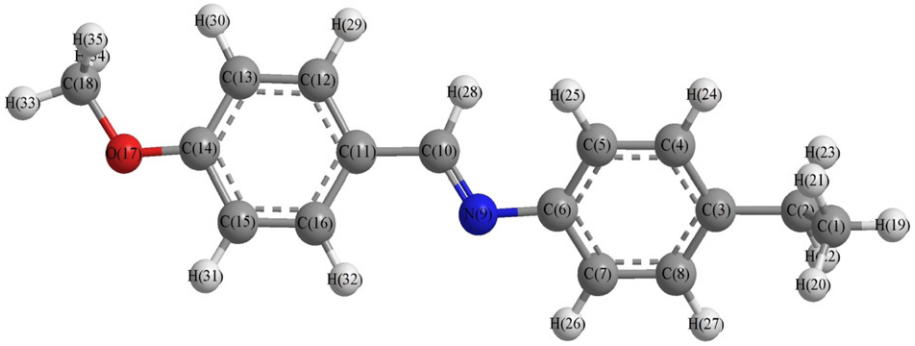

Fig. 1. Molecular geometry of MBEA liquid crystal.

Table 1
Calculated bond lengths (Å), bond angles (°) and dihedral angles (°) of MBEA molecule.

Bond length	HF/6-31G(d,p)	B3LYP/6-31G(d,p)	Bond angle	HF/6-31G(d,p)	B3LYP/6-31G(d,p)
C(18)-O(17)	1.399	1.421	C(14)-O(17)-C(18)	119.88	118.25
O(17)-C(14)	1.343	1.362	C(11)-C(16)-C(15)	120.63	120.69
C(16)-C(11)	1.400	1.383	C(16)-C(15)-C(14)	120.33	120.22
C(16)-C(15)	1.370	1.409	O(17)-C(14)-C(15)	115.66	115.58
C(15)-C(14)	1.399	1.407	O(17)-C(14)-C(13)	124.56	124.60
C(14)-C(13)	1.383	1.401	C(15)-C(14)-C(13)	119.76	119.80
C(13)-C(12)	1.389	1.394	C(14)-C(13)-C(12)	119.14	119.30
C(12)-C(11)	1.381	1.399	C(13)-C(12)-C(11)	121.74	121.47
C(11)-C(10)	1.470	1.462	C(10)-C(11)-C(16)	122.16	121.73
C(10)-N(9)	1.256	1.282	C(10)-C(11)-C(12)	119.46	119.75
N(9)-C(6)	1.408	1.406	C(16)-C(11)-C(12)	118.36	118.50
C(8)-C(3)	1.389	1.392	N(9)-C(10)-C(11)	123.12	122.65
C(8)-C(7)	1.384	1.401	C(6)-N(9)-C(10)	120.41	119.93
C(7)-C(6)	1.389	1.403	C(3)-C(8)-C(7)	121.32	121.36
C(6)-C(5)	1.392	1.407	C(8)-C(7)-C(6)	120.68	120.55
C(5)-C(4)	1.381	1.391	N(9)-C(6)-C(7)	117.71	117.75
C(4)-C(3)	1.390	1.402	N(9)-C(6)-C(5)	123.88	123.76
C(3)-C(2)	1.514	1.514	C(7)-C(6)-C(5)	118.35	118.45
C(2)-C(1)	1.532	1.539	C(6)-C(5)-C(4)	120.48	120.40
			C(5)-C(4)-C(3)	121.52	121.44
			C(2)-C(3)-C(8)	121.67	121.34
			C(2)-C(3)-C(4)	120.69	120.86
			C(8)-C(3)-C(4)	117.60	117.75
			C(1)-C(2)-C(3)	113.46	112.95

Dihedral angle	HF/6-31G(d,p)	B3LYP/6-31G(d,p)	Dihedral angle	HF/6-31G(d,p)	B3LYP/6-31G(d,p)
C(18)-O(17)-C(14)-C(13)	0.51	1.02	C(10)-N(9)-C(6)-C(5)	35.36	34.60
C(18)-O(17)-C(14)-C(15)	−179.55	−178.93	C(10)-N(9)-C(6)-C(7)	−146.95	−147.26
C(15)-C(16)-C(11)-C(12)	0.19	−0.11	C(7)-C(8)-C(3)-C(4)	−0.57	1.28
C(15)-C(16)-C(11)-C(10)	−179.71	0.14	C(7)-C(8)-C(3)-C(2)	177.64	−0.34
C(11)-C(16)-C(15)-C(14)	0.02	−179.41	C(3)-C(8)-C(7)-C(6)	0.87	177.32
C(16)-C(15)-C(14)-C(13)	−0.24	0.02	C(8)-C(7)-C(6)-C(5)	−1.11	−1.69
C(16)-C(15)-C(14)-O(17)	179.81	179.98	C(8)-C(7)-C(6)-N(9)	−178.93	−179.92
C(15)-C(14)-C(13)-C(12)	0.23	0.02	C(7)-C(6)-C(5)-C(4)	1.11	1.22
O(17)-C(14)-C(13)-C(12)	−179.82	−179.93	N(9)-C(6)-C(5)-C(4)	178.78	179.34
C(14)-C(13)-C(12)-C(11)	−0.01	0.01	C(6)-C(5)-C(4)-C(3)	−0.86	−0.32
C(13)-C(12)-C(11)-C(16)	−0.20	−0.08	C(5)-C(4)-C(3)-C(8)	0.57	−0.13
C(13)-C(12)-C(11)-C(10)	179.70	179.47	C(5)-C(4)-C(3)-C(2)	−177.66	−177.81
C(12)-C(11)-C(10)-N(9)	−179.01	−179.00	C(4)-C(3)-C(2)-C(1)	72.44	72.40
C(16)-C(11)-C(10)-N(9)	0.90	0.54	C(8)-C(3)-C(2)-C(1)	−105.72	−105.19
C(11)-C(10)-N(9)-C(6)	−178.50	−179.74			

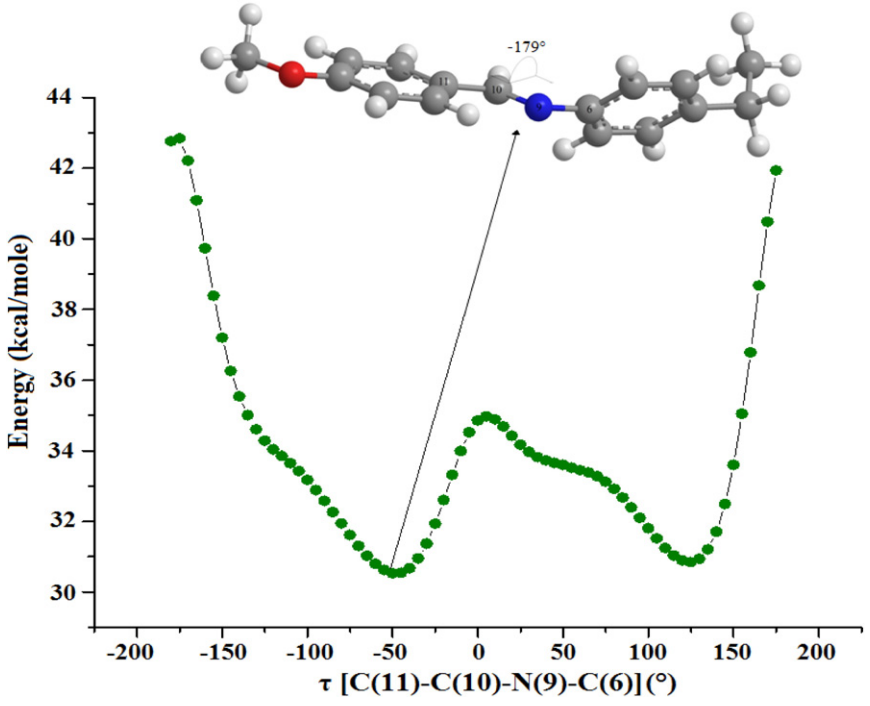

Fig. 2. Variation of potential energy of MBEA molecule as a function of the torsion angle τ.

corresponding bond lengths and bond angles are given in Table 1. Rotational flexibility of the MBEA molecule at the middle and its terminal involving methoxy group has been examined with the help of conformational analysis that has been carried by DFT technique. The potential energy variation relative to the torsion angle τ, with resolution of 10^0, as depicted in Fig. 2, shows that MBEA molecule exhibits one stable conformer. The global energy minimum of the *trans–trans* conformer is obtained at $\tau = -50^0$. The energy corresponding to this angle is 30.52 kcal/mole. Another local minimum is obtained at $\tau = 125^0$. Further, one global maximum or *cis cis* conformer is obtained at -175^0 with the energy value of 42.84 kcal/mole.

The potential energy surface for the two torsion angles τ_1 and τ_2, with resolution of 10^0 at the terminal end shows that MBEA molecule exhibits its several stable conformers (dark blue regions) which are in the *trans–trans* conformations (Fig. 3). Energy minimization or the global minimum of the *trans–trans* conformer of MBEA molecule is obtained at $\tau_1 = -60^0$ and $\tau_2 = 0^0$. The corresponding minimum energy is 33.81 kcal/mole. The global maximum or *cis–cis* (red region) conformer is obtained at $\tau_1 = 120^0$ and $\tau_2 = -180^0$ with energy of 73.20 kcal/mole. There are five other local maxima positions corresponding to (i) $\tau_1 = -120^0$ and $\tau_2 = -180^0$, (ii) $\tau_1 = -110^0$ and $\tau_2 = 170^0$, (iii) $\tau_1 = 0^0$ and $\tau_2 = -180^0$, (iv) $\tau_1 = 10^0$ and $\tau_2 = 170^0$ and (v) $\tau_1 = 130^0$ and $\tau_2 = 170^0$ which indicate that these molecular conformations are energetically unfavoured.

Mulliken population analysis (MPA) of MBEA molecule has been carried out at HF/6-31G(d,p) and B3LYP/6-31G(d,p) levels. Table 2 shows the partial charges located on the various atoms of the MBEA molecule. As evident from Table 2, electronegative atoms like nitrogen and oxygen always possess negative charge. Hydrogen atoms bear electropositive charge irrespective of their position in the molecule. However, carbon atoms assume both positive and negative charge according to their positions in the molecule (Fig. 4).

Table 2
Mulliken's atomic charge of MBEA molecule.

Atom no.	Atom symbol	Atomic charge (e.u.)	
		HF/6-31G(d,p)	B3LYP/6-31G(d,p)
1	C	−0.322	−0.307
2	C	−0.229	−0.242
3	C	−0.009	0.137
4	C	−0.152	−0.135
5	C	−0.155	−0.091
6	C	0.214	0.238
7	C	−0.139	−0.088
8	C	−0.161	−0.136
9	N	−0.575	−0.484
10	C	0.199	0.117
11	C	−0.098	0.091
12	C	−0.135	−0.141
13	C	−0.228	−0.138
14	C	0.421	0.354
15	C	−0.191	−0.113
16	C	−0.100	−0.103
17	O	−0.657	−0.504
18	C	−0.031	−0.078
19	H	0.110	0.100
20	H	0.119	0.110
21	H	0.113	0.107
22	H	0.119	0.097
23	H	0.122	0.103
24	H	0.142	0.073
25	H	0.148	0.079
26	H	0.160	0.086
27	H	0.144	0.074
28	H	0.126	0.067
29	H	0.155	0.082
30	H	0.156	0.085
31	H	0.169	0.095
32	H	0.191	0.109
33	H	0.142	0.126
34	H	0.116	0.112
35	H	0.115	0.112

3.2. Molecular electrostatic potential (MEP) and HOMO–LUMO surface analysis

MEP can be employed as an informative tool to describe different physical and chemical features, non-covalent interactions, proton affinities, solvation process and also in the evaluation of electrostatic charges for molecular mechanics and molecular dynamics studies. However, nucleophilic reaction happens more easily in the most negative area of MEP and electrophilic reaction happens more easily in the most positive area of the MEP. As evident from Fig. 5, electron densities are very low at the outer surface and near the hydrogen atoms (blue and light blue regions). Hence electrostatic potentials near these regions are positive. In the inner surface of the molecule (yellow and green regions), electron

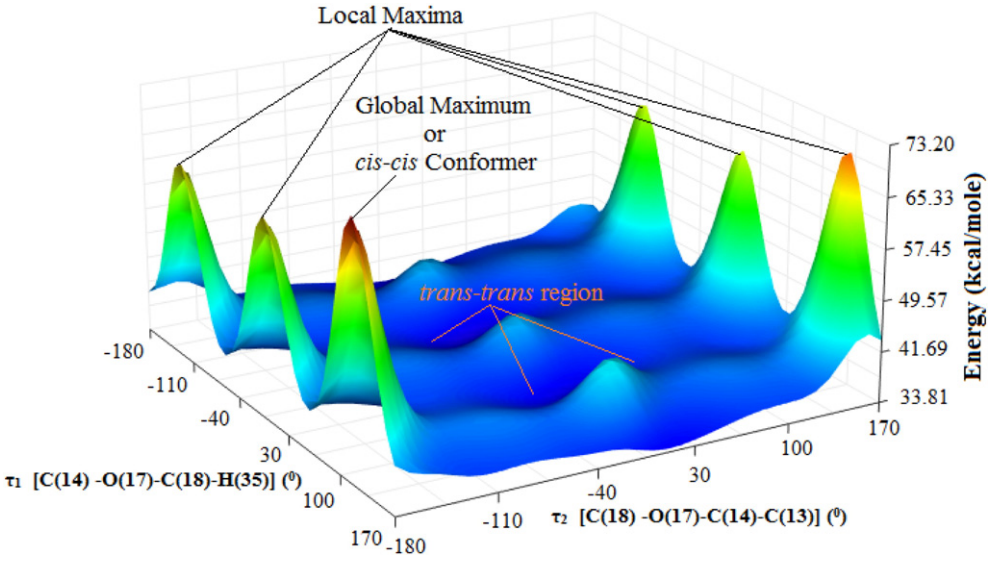

Fig. 3. Surface plot of the relative potential energy of MBEA molecule as a function of the two constitutive torsion angles τ_1 and τ_2.

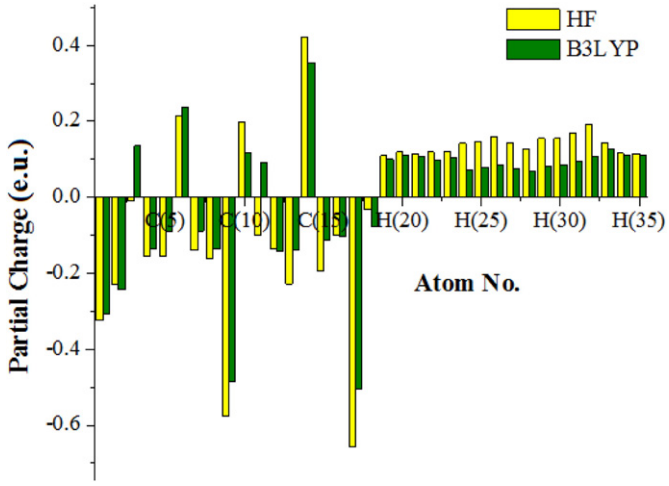

Fig. 4. Mulliken plot of MBEA liquid crystal molecule.

densities are on average high due to the presence of carbon atoms which have less electronegativity. Hence the electrostatic potential is less negative near these regions. The electron densities are very high at the centre and at one end of the molecule (red regions). This is due to the presence of strong electronegative atoms such as oxygen at terminal and nitrogen in the central linkage group. Thus, the MEP map shows negative potential sites on oxygen and nitrogen atoms while positive potential sites are around the hydrogen atoms (Fig. 5), which is useful for the analysis of intermolecular potential between a pair of MBEA molecules.

HOMO and LUMO of the MBEA molecule are shown in Fig. 6. The dominance of the functional groups can easily be visualised. The

Table 3
Electronic properties and global parameters of MBEA molecule.

Global parameters	HF/6-31G(d,p)	B3LYP/6-31G(d,p)
HOMO energy	−0.279 a.u.	−0.198 a.u.
LUMO energy	0.094 a.u.	−0.044 a.u.
Orbital energy gap (ΔE)	0.373 a.u.	0.154 a.u.
Ionization potential (I)	0.279 a.u.	0.198 a.u.
Electron affinity (A)	−0.094 a.u.	0.044 a.u.
Electronegativity (χ)	0.092 a.u.	0.121 a.u.
Electronic chemical potential (μ)	−0.092 a.u.	−0.121 a.u.
Global hardness (η)	0.186 a.u.	0.077 a.u.
Global softness (S)	5.376 $a.u.^{-1}$	12.987 $a.u.^{-1}$
Electrophilicity index (ω)	0.022 a.u.	0.095 a.u.

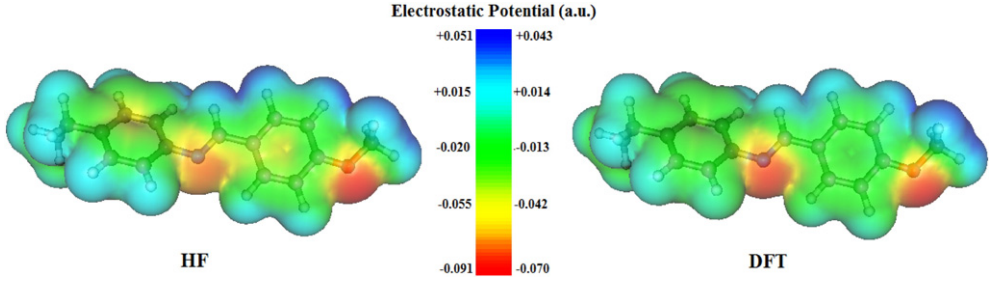

Fig. 5. The molecular electrostatic potential surface of MBEA molecule projected on 0.001 electrons/$bohr^3$ isodensity surface.

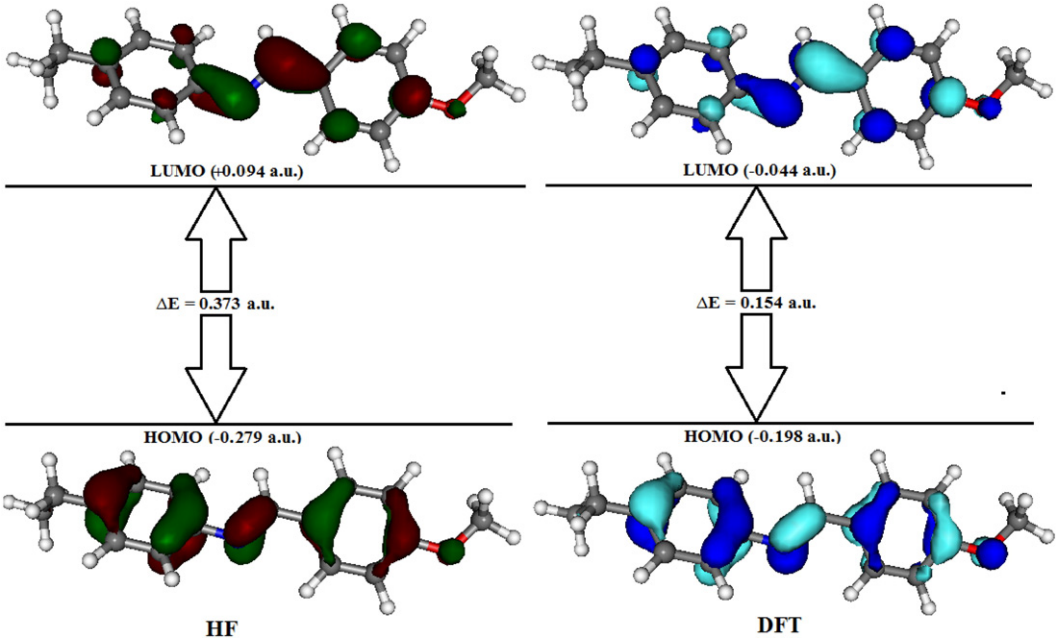

Fig. 6. HOMO and LUMO of the MBEA liquid crystal molecule.

Table 4
Thermodynamical parameters of MBEA molecule.

Parameters	HF/6-31G(d,p)	B3LYP/6-31G(d,p)
Specific heat at constant pressure (C_p)	60.81 cal/(mol K)	63.36 cal/(mol K)
Specific heat at constant volume (C_v)	58.82 cal/(mol K)	61.38 cal/(mol K)
Enthalpy	206.37 kcal/mol	193.76 kcal/mol
Entropy	130.46 cal/(mol K)	128.34 cal/(mol K)
Gibbs free energy	167.47 kcal/mol	155.49 kcal/mol
Internal energy	205.78 kcal/mol	193.17 kcal/mol
Kinetic energy	467,104.22 kcal/mol	466,057.33 kcal/mol
Total energy	−467,569.38 kcal/mol	−470,293.63 kcal/mol
Dipole moment	3.06 Debye	2.94 Debye

valence orbitals are largely delocalized. The HOMO of the molecule is highly centred on both phenyl rings involving carbon atoms 4, 3, 8, and 5, 6, 7, in one ring, while 12, 11, 16, and 13, 14, 15 in the other ring. The linkage C═N group which is also highly occupied, is shortened due to the complete overlap of electron densities. Also the oxygen atom is occupied at the terminal of the molecule. On the other hand, in LUMO, there is a delocalization of valence (virtual) orbitals throughout the molecule. Nitrogen atom of the linkage group overlap one of the carbon atoms of the adjacent phenyl ring while other carbon atom of the linkage group is overlapped with carbon atom of other phenyl ring. Further, in LUMO, carbon atoms of both the phenyl rings and oxygen atom at terminal are individually less occupied. The ionization potential, electron affinity, electronegativity, global hardness and softness, total energy, dipole moment and HOMO–LUMO energy gap (ΔE) of MBEA molecule are given in Table 3. The thermodynamical parameters, which are computed at 298.15 K temperature, are listed in Table 4.

3.3. IR spectra analysis

The vibrational spectral analysis of MBEA molecule is performed on the basis of the characteristic vibrations of the ethyl group and methyl group. The vibrational assignments contain various modes including the CH stretching modes of CH_3 groups, CH_3 deformations, and CC skeletal vibrations along with HCC bending vibrations [33–35]. Theoretically calculated vibrational (IR) frequencies of MBEA have been compared with the experimental observations in Table 5 while the corresponding spectrum is presented in Fig. 7.

Table 5
Vibrational assignments of MBEA molecule.

Experimental frequency/cm^{-1}	Theoretical frequency/cm^{-1} and corresponding Intensities				Assignments
	HF/6-31G(d,p)	Intensity (km/mol)	B3LYP/6-31G(d,p)	Intensity (km/mol)	
411	462.48	2.31	421.95	1.63	Ring out of plane deformation
	473.14	4.53	427.37	1.47	
474	482.64	0.68	493.58	5.52	
527	527.96	3.07	540.53	3.00	
551	555.18	11.91	573.07	14.97	
	590.40	3.28	605.12	19.59	
637	644.87	20.49	–	–	
	–	–	–	–	
650	697.16	1.44	654.57	1.77	
	706.10	0.95	662.93	0.56	
776	798.75	4.21	788.2	2.89	C—H out of plane bending
807	818.49	1.38	801.12	1.88	
824	845.23	2.21	856.48	47.92	
885	913.25	1.49	973.9	0.97	CH_3 rocking
1003	949.12	62.77	1011.63	8.66	Inter ring C—C stretching
1019	–	–	1032.99	0.24	C—C stretching
	–	–	1038.11	4.43	
1061	1064.49	0.52	1071.50	66.53	
1121	1114.6	0.34	1134.84	29.79	In-plane ring HCC bending
	1132.17	2.85	1144.02	7.76	
1179	1180.20	68.81	1198.16	109.26	
	1205.76	18.78	1201.9	12.48	
1250	1300.29	15.07	1298.24	414.05	In-plane ring HCC bending + COC stretching
1287	1283.47	115.16	1284.34	43.39	
1314	1325.75	27.36	1330.75	3.79	
	1334.04	148.15	1341.63	45.46	
1348	–	–	1350.04	9.12	
	–	–	1368.06	37.02	
1374	1371.32	8.23	1422.5	1.13	CH_3 umbrella deformation
	1437.43	322.38	–	–	
1456	1455.32	1.57	1486.52	22.17	
	1488.42	15.77	1499.78	5.32	
1522	1533.65	11.65	1549.57	14.05	Ring CC stretching
	1574.35	14.53	1565.35	131.19	
1605	1617.69	5.27	1619.23	11.71	
	1692.68	217.43	1622.55	129.05	
1663	1902.97	348.69	1673.57	145.43	C═N stretching
2866	3181.49	64.01	3003.05	82.64	Symmetric CH stretch of (CH_3)
2964	3246.42	74.43	3131.67	54.79	Asymmetric CH stretch of (CH_3)
3032	3332.39	28.04	3182.74	52.04	Aromatic CH stretching
3070	3393.89	6.47	3219.95	11.85	

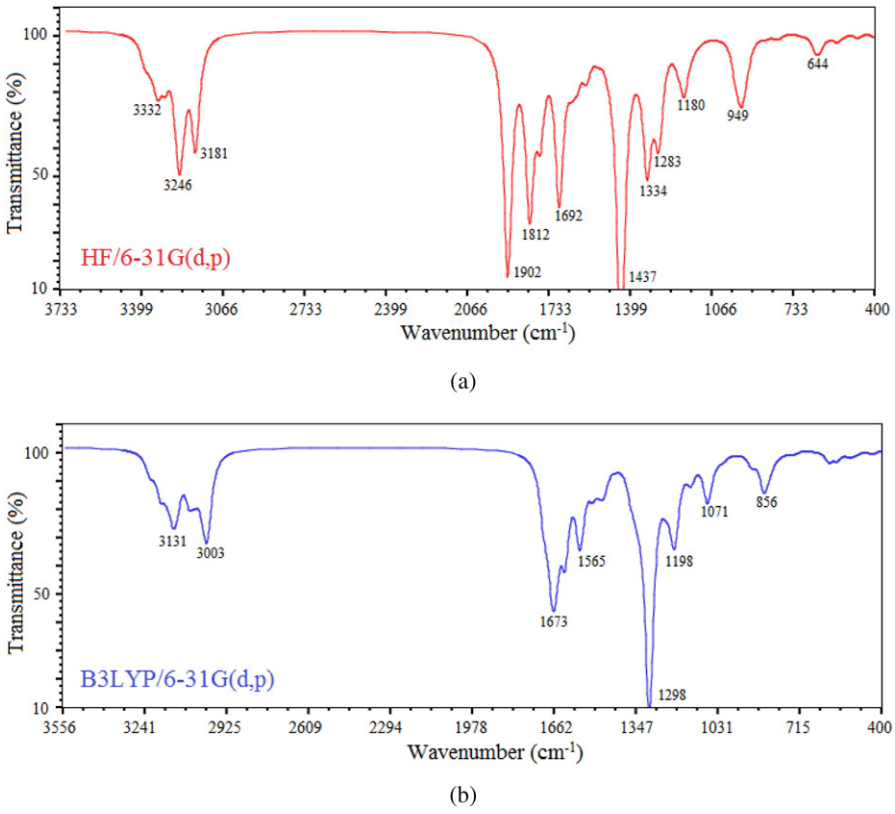

Fig. 7. IR spectrum of MBEA liquid crystal molecule as observed from quantum mechanical calculations: (a) ab-initio and (b) DFT technique.

3.3.1. CH stretching vibration

DFT and ab-initio methods yield CH stretching vibrations in the range from 3003 cm^{-1} to 3219 cm^{-1} and 3178 cm^{-1} to 3393 cm^{-1} respectively. The experimental CH stretching vibrations lie in the region from 2849 cm^{-1} to 3070 cm^{-1}. Methyl group vibrations are generally referred to as electron donating substituent in the aromatic rings system [36,37]. The asymmetric CH stretching mode of CH_3 is expected around 2964 cm^{-1} and the CH_3 symmetric stretching is expected at 2866 cm^{-1}. The CH symmetric and asymmetric stretching vibrations of methyl group which arises due to aromatic moiety are also available in this region. Theoretically computed CH symmetric and asymmetric vibrations of methyl appear at 3003 cm^{-1} and 3070 cm^{-1} respectively in DFT method while the same appear at 3178 cm^{-1} and 3259 cm^{-1} respectively in ab-initio method. The experimental aromatic stretching modes are observed at 3032 cm^{-1} and 3070 cm^{-1} while corresponding theoretical values lie at 3182 cm^{-1} and 3229 cm^{-1} respectively.

3.3.2. C═N stretching vibration

The C═N stretching vibration occurs in the region between 1613 and 1663 cm^{-1} [38]. This vibration observed at 1902 cm^{-1} in ab-initio and at 1703 cm^{-1} in DFT calculation.

3.3.3. Ring and other vibrations

Vibrations like inter ring CH out of plane bending, inter ring C—C stretching, C—C stretching and in-plane ring HCC bending modes are also observed in aromatic moieties. These vibrations are observed at 788, 1011, 1032, and 1134 cm^{-1} respectively while CH_3 rocking mode appears at 973 cm^{-1}. CH_3 umbrella deformation is observed at 1422 cm^{-1}. Ring CC stretching lies in the range from 1549 to 1622 cm^{-1}.

As evident from Table 5, theoretically computed values of vibrational modes using ab-initio and/or DFT method, are in good agreement with experimental data. It seems pertinent to mention that the B3LYP method has been found to be equivalent to or even better than HF method [39].

3.4. Interaction energy analysis

Using the net charge and corresponding dipole components as computed by DFT technique, intermolecular interactions between a pair of MBEA molecules have been evaluated. All possible interacting configurations have been taken into account. Nature and strength of various types of interactions have been examined. Results obtained in different molecular configurations are discussed as under.

3.4.1. Stacking interaction

The interplanar distance between the MBEA molecules has been varied in the range of ± 12.0 Å an interval of ± 0.5 Å. Dependence of stacking energy on interplanar separation along +*Z*-axis is shown in Fig. 8. Stacking minimum with energy of − 3.96 kcal/mole is obtained at an interplanar separation of 4.5 Å corresponding to which angular dependence of stacking energy has been examined. As evident from Fig. 9, four minima with energy values of − 7.36, − 7.87, − 7.79 and − 8.68 kcal/mole are obtained when relative orientation between MBEA molecules becomes 30^0, 170^0, 190^0 and 210^0 respectively. Since the configuration with energy of − 8.68 kcal/mole at 210^0 corresponds to lower value, it has been chosen for analyzing the translational freedom of molecules in the stacked pair. Further, it is observed that electrostatic and

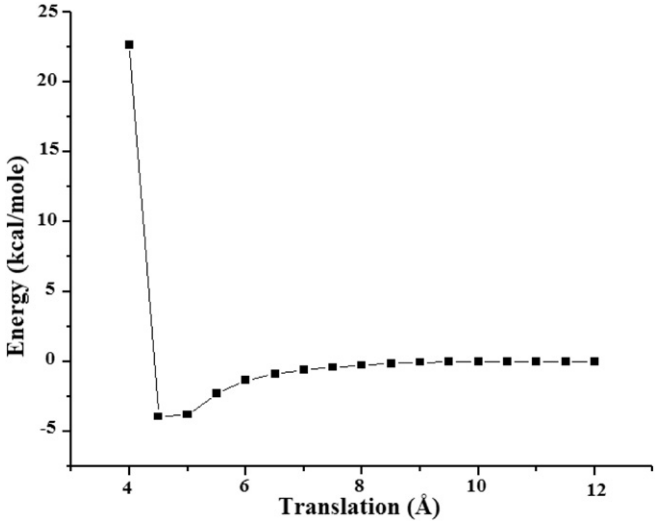

Fig. 8. Variation of total stacking energy with respect to translation of one of the stacked MBEA molecules along +Z axis.

polarization components are very weak while dispersion energy term contributes significantly to the stability of complexes. The variation of stacking energy with respect to translation along ±X-axes has been shown in Fig. 10. As evident from this figure, for translations in the range of ±2.0 Å, small change in the energy (less than 1.0 kcal/mole) of stacked complexes is noticed; which indicates that one of the stacked MBEA molecules can slide over the other in the range of ±2.0 Å along its long molecular axis without any significant loss of energy. The stacked minimum energy complex possesses energy of −12.29 kcal/mole at an interplanar separation of 3.9 Å (configuration-1). Likewise during translation along –*Z*-axis, minimum energy stacked complex corresponds to the energy of −11.87 kcal/mole with an interplanar separation of 4.0 Å (configuration-2).

3.4.2. In–plane (side to side) interaction

During in–plane (side to side) interactions, one of the interacting molecules has been placed at a distance of 11.0 Å along the ±Y-axis and translations have been introduced at an interval of 0.5 Å. Variation of interaction energy is shown in Fig. 11. As evident from this figure, energy between the two MBEA molecules is minimized at an intermolecular distance of 6.0 Å with the energy of −5.30 kcal/mole. Further, refinement of the in-plane (side to side) configurations have been done at the interval of 0.1 Å along both ±X and ±Y-axes so as to find out the minimum energy configurations. The configuration–1 is obtained when one of the MBEA molecules is displaced along +Y-axis while configuration −2 is obtained when one of the MBEA molecules is displaced along –Y–axis keeping the other fixed. The minimum energy configurations are stabilized with energy of −8.42 kcal/mole and −8.79 kcal/mole at the separation of 7.1 Å (configuration-1) and 6.9 Å (configuration-2) respectively.

3.4.3. In–plane (end to end) interaction

The MBEA molecule consists of methoxy group at one end while ethyl group at the other end. All possible interacting configurations between the terminal groups have been considered. One of the MBEA molecules is placed at the terminal end of the other and translations are introduced at the interval of 0.5 Å in the range of ±25.0 Å. The energy minimum, thus obtained, is subjected to refinement at an interval of 0.1 Å. The variation of total interaction energy during terminal interactions is shown in Fig. 12. The energy curve shows minimum having energy of −2.01 kcal/mole when centre of mass positions of the two interacting MBEA molecules are separated by 16.5 Å. The terminal interaction energy remains almost constant in the range from 16.4 to 16.6 Å. However, a slight decrease or increase in the end to end separation causes sharp changes in the interaction energy. Total energy and its components during stacking, in-plane (side to side) and terminal (end to end) interactions are listed in Table 6. As evident from this table,

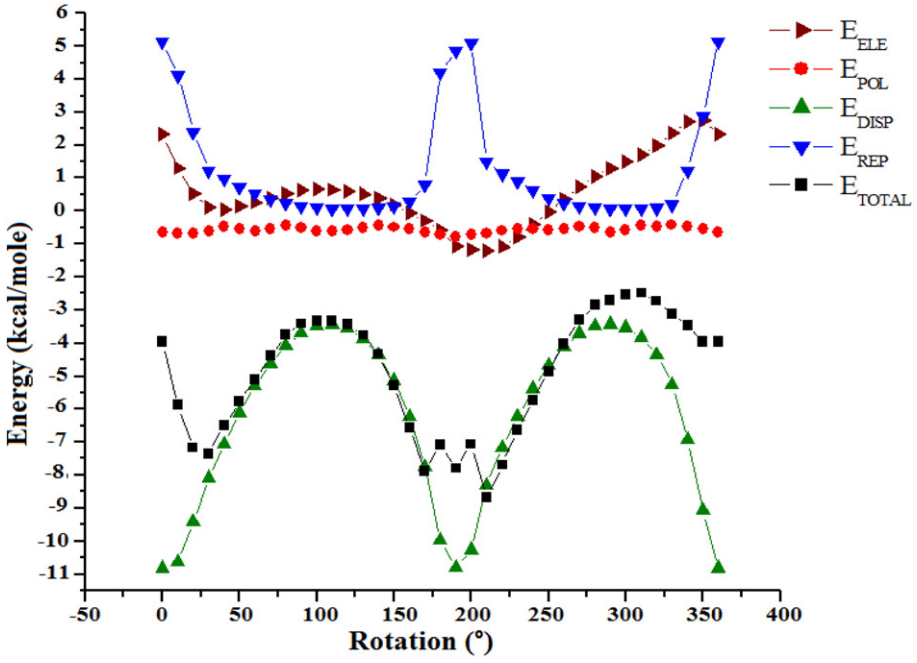

Fig. 9. Variation of total stacking energy and its components with respect to rotation of one of the stacked MBEA molecules about +Z axis.

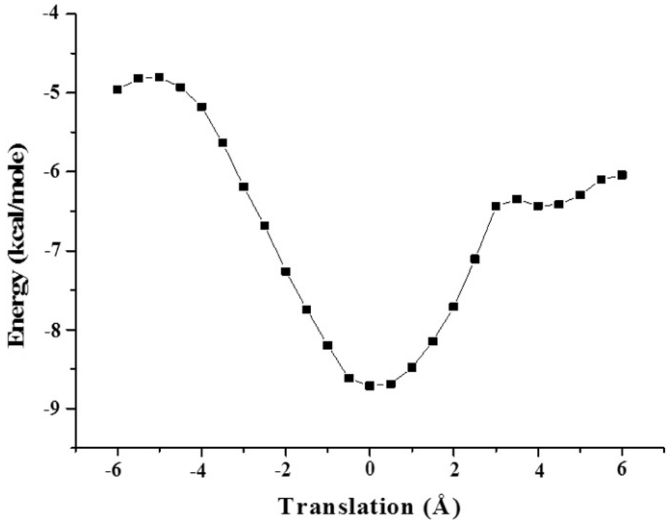

Fig. 10. Variation of total stacking energy with respect to translation of one of the stacked MBEA molecules along ±X-axis. The minimum energy corresponds to −8.71 kcal/mole at X = 0 Å.

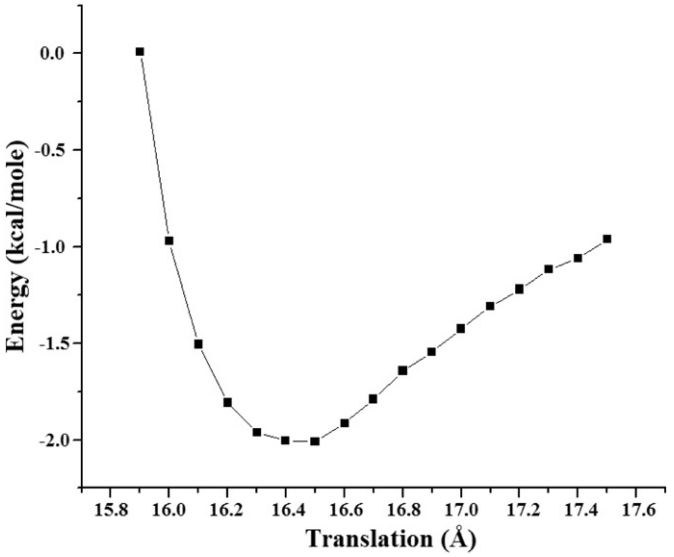

Fig. 12. Variation of total energy during terminal interactions between methoxy group of one and ethyl group of the other MBEA molecule (after refinement).

electrostatic and polarization components are very weak while dispersion components play dominant role in stabilizing the intermolecular complexes. This is in accordance with the Maier-Saupe theory [40] and other observations [16,41]. Further, weaker terminal energy as compared to stacking and in-plane energies favour the nematic behaviour of MBEA molecules. Minimum energy configurations resulting from stacking, in-plane and end to end interactions (for configuration-1 only) are shown in Fig. 13.

4. Conclusion

Conformational analysis suggests that dihedral angle involving atoms C(11), C(10), N(9) and C(6) at the central linkage group of MBEA molecule is −179°, which corresponds to a good stable conformer. The MEP and HOMO-LUMO analysis may be used to predict accurately chemical reactivity, charge transfer and electrostatic properties of the MBEA molecule. The MEP surface of the MBEA molecule is asymmetric in nature. The thermochemistry measured at 298.15 K suggests that certain chemical reactions may take place inside the system in which either heat is released or absorbed. Calculated vibrational frequencies of various functional groups of the para-methoxybenzylidine *p*-ethylaniline molecule are in good agreement with experimental data available in literature. Major contribution to the stability of the stacked and in-plane (side to side) or terminal configurations is due to dispersion (induced dipole-induced dipole) type of interactions. Further, molecules of MBEA in a stacked pair exhibit translational freedom and also orientational flexibility which may further increase at higher temperatures. In the stacked pair, molecules possess a relative orientation of 180^0 i.e. antiparallel configuration. These results favour the nematic behaviour of the system.

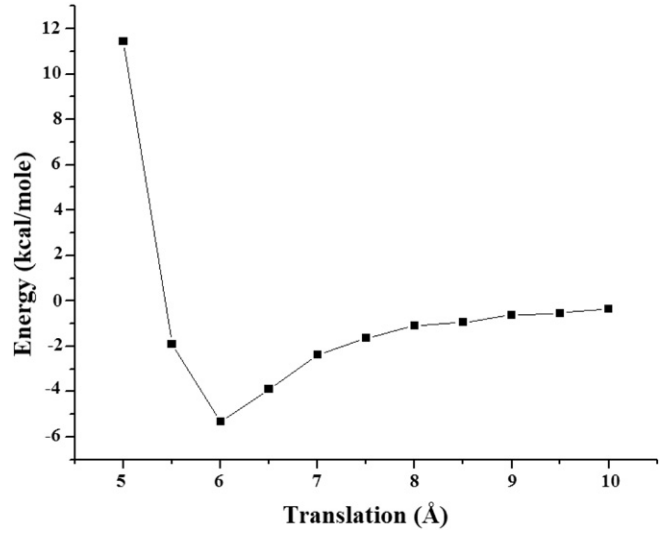

Fig. 11. Variation of total energy with respect to translation of one of the interacting MBEA molecules along +Y-axis during in-plane (side to side) interactions.

Acknowledgements

Authors are thankful to Dr. Mark S. Gordon, Department of Chemistry, Iowa State University for providing us the GAMESS program, August 2013.

Table 6
Interaction energy components corresponding to minimum energy configurations of MBEA molecules during stacking, in-plane (side to side) and terminal (end to end) interactions. Energy is expressed in kcal/mole.

Energy terms	Stacking interactions		In-plane (side to side) interactions		Terminal (end to end) interactions	
	Conf. 1	Conf. 2	Conf. 1	Conf. 2	Conf. 1	Conf. 2
E_{QQ}	−1.24	−1.10	−1.43	−2.31	−0.21	−0.21
E_{QMI}	−0.74	−0.78	−0.61	0.03	−0.42	−0.29
E_{MIMI}	−0.02	−0.02	0.03	−0.01	0.01	0.01
E_{ELE}	−2.00	−1.90	−2.01	−2.29	−0.62	−0.49
E_{POL}	−1.16	−1.13	−0.86	−0.53	−0.21	−0.20
E_{DISP}	−16.76	−15.11	−8.84	−11.36	−2.18	−2.18
E_{REP}	7.62	6.27	3.29	5.39	1.00	1.00
E_{TOTAL}	−12.29	−11.87	−8.42	−8.42	−2.01	−1.87

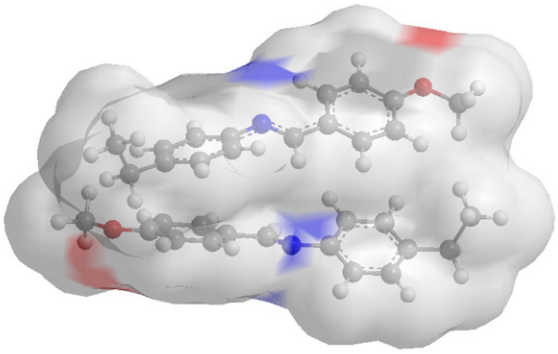

Stacking interaction (-12.29 kcal/mole)

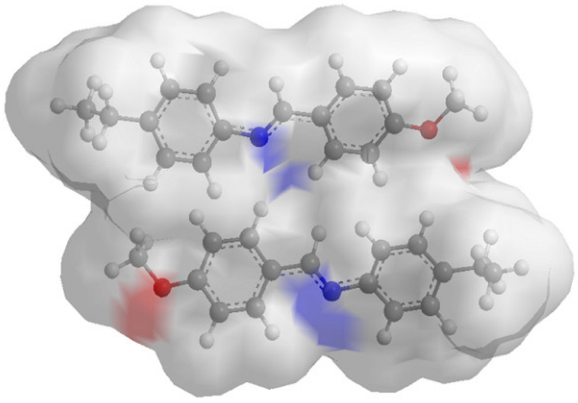

In-plane interaction (-8.42 kcal/mole)

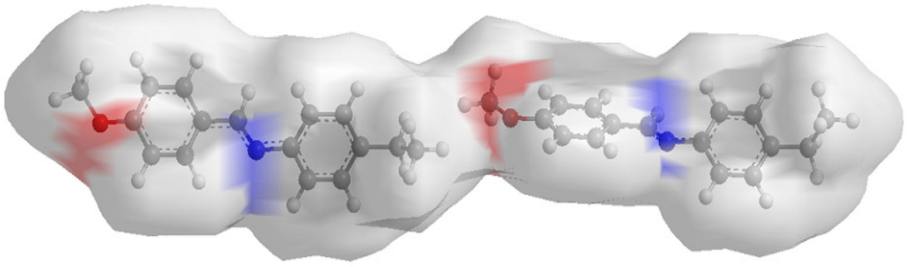

Terminal interaction (-2.01 kcal/mole)

Fig. 13. Minimum energy configurations of MBEA molecules during stacking, in-plane (side to side) and terminal interactions in configuration-1. Energy decomposition is given in Table 6.

References

[1] V. Milman, et al., Int. J. Quantum Chem. 77 (2000) 895.
[2] M. Sob, M. Friak, D. Legut, J. Fiala, V. Vitek, Mater. Sci. Eng. A 387 (2004) 148.
[3] V.D. Teodoro, R.G. Neves, Comput. Phys. Commun. 182 (2011) 8.
[4] S. Chandrasekhar, Liquid Crystals, Cambridge University Press, London, 1992.
[5] P.G. de Gennes, The Physics of Liquid Crystals, Clarendon Press, Oxford, 1993.
[6] G.H. Brown, J. Chem. Educ. 60 (1983) 901–905.
[7] B. Bahadur (Ed.), Liquid Crystals: Application and Uses, Vols. I, II and III, World Scientific, Singapore, 1990.
[8] G.W. Gray, Molecular Structure and Properties of Liquid Crystals, Academic Press, New York, 1962.
[9] D. Sharma, S.N. Tiwari, J. Mol. Liq. 214 (2016) 128–135.
[10] M. Mishra, M.K. Dwivedi, R. Shukla, S.N. Tiwari, Prog. Cryst. Growth Charact. Mater. 52 (2006) 114–124.
[11] K.K. Dwivedi, M.K. Dwivedi, S.N. Tiwari, J. Cryst. Proc. Technol. 4 (2014) 31–38.
[12] S. Chaturvedi, N. Chaturvedi, M.K. Dwivedi, S.N. Tiwari, Indian J. Phys. 87 (2013) 263–269.
[13] M.K. Dwivedi, S.N. Tiwari, J. Mol. Liq. 158 (2011) 208–211.
[14] A.M. Smondyrev, R.A. Phcovtis, Liq. Cryst. 26 (1999) 235–240.
[15] G.R. Luckhurst, S. Romono, Liq. Cryst. 26 (1999) 871–884.
[16] S.N. Tiwari, D. Sharma, J. Mol. Liq. 207 (2015) 99–106.
[17] S.H. Vosco, L. Wilk, M. Nusair, Can. J. Phys. 58 (1980) 1200–1211.
[18] J.M. Campanario, E. Bronchalo, M.A. Hidalgo, J. Chem. Educ. 71 (1994) 761–766.
[19] I.N. Levine, Quantum Chemistry, fifth ed Pearson Education, Singapore, 2003.
[20] M.W. Schmidt, et al., J. Comput. Chem. 14 (1993) 1347–1363.
[21] E. Scrocco, J. Tomasi, Top. Curr. Chem. 42 (1973) 95–170.
[22] N.H. March, J. Theor. Comput. Chem. 3 (1996) 619–647.
[23] R.G. Parr, R.A. Donnelly, M. Levy, W.E. Palke, J. Chem. Phys. 68 (1978) 3801–3807.
[24] P. Geerlings, F. De Proft, W. Langenaeker, Chem. Rev. 103 (2003) 1793.
[25] J.B. Foresman, A. Frisch, Exploring Chemistry with Electronic Structure Methods, second ed Gaussian, Inc., Pittsburg, 1996.
[26] L. Pauling, The Nature of the Chemical Bond, Cornell University Press, Ithaca, New York, 1960.
[27] P. Senet, Chem. Phys. Lett. 275 (1997) 527–532.
[28] R.G. Parr, L. Szentpaly, S. Liu, J. Am. Chem. Soc. 121 (1999) 1922–1924.
[29] P. Claverie, in: B. Pullman (Ed.), Intermolecular Interactions: From Diatomics to Biopolymers, John Wiley, New York 1978, pp. 69–305.
[30] R. Rein, in: B. Pullman (Ed.), Intermolecular Interactions: From Diatomics to Biolymers, John Wiley, New York 1978, pp. 307–362.
[31] R. Rein, Adv. Quantum Chem. 7 (1973) 335–396.
[32] J. Langlet, P. Claverie, F. Caron, J.C. Boeuve, Int. J. Quantum Chem. 20 (1981) 299–338.
[33] R.G. Snyder, J.R. Scherer, J. Chem. Phys. 71 (1979) 3221;
R.G. Snyder, M. Maroncelli, H.L. Strauss, J. Am. Chem. Soc. 105 (1983) 133;
R.G. Snyder, V.J.P. Srivatsavoy, D.A. Cates, H.L. Strauss, J.W. White, D.L. Darset, J. Phys. Chem. 98 (1994) 674.

[34] M. Maroncelli, S.P. Qi, H.L. Strauss, R.G. Snyder, J. Am. Chem. Soc. 104 (1982) 6237;
M. Maroncelli, H.L. Strauss, R.G. Snyder, J. Phys. Chem. 89 (1985) 5260;
M. Maroncelli, H.L. Strauss, R.G. Snyder, J. Phys. Chem. 82 (1985) 2811.
[35] L.M. Barbkov, I.I. Gnatyuk, S.V. Trukhachev, J. Mol. Struct. 744 (2005) 425–432.
[36] D. Sajan, I. Hubert Joe, V.S. Jayakumar, J. Raman, Spectroscopy 37 (2005) 508–519.
[37] M. Gussoni, C. Castiglioni, M.N. Ramos, M.C. Rui, G. Zerbi, J. Mol. Struct. 224 (1990) 445–449.
[38] L. Clougherty, J. Sousa, G. Wyman, J. Org. Chem. 22 (1957) 462.
[39] A.K. Srivastava, N. Misra, Chem. Phys. Lett. 612 (2014) 302–305.
[40] W. Maier, A. Saupe, Z. Naturforsch. 13A (1958) 564–566;
W. Maier, A. Saupe, Z. Naturforsch. 14A (1959) 882–889;
W. Maier, A. Saupe, Z. Naturforsch. 15A (1960) 287–292.
[41] J.W. Baran, A. Les, Mol. Cryst. Liq. Cryst. 54 (1979) 273–288.